Green Chemistry

PAPER

View Article Online
View Journal | View Issue

Cite this: *Green Chem.*, 2020, **22**, 6212

Phosphorescent bio-based resin for digital light processing (DLP) 3D-printing†

Mirko Maturi, Carolina Pulignani, Erica Locatelli, Veronica Vetri Buratti, Silvia Tortorella, Letizia Sambri and Mauro Comes Franchini *

Received 11th June 2020,
Accepted 18th August 2020

DOI: 10.1039/d0gc01983f

rsc.li/greenchem

Since the advent of polymer-based 3D printing technology, the scientific community has directed great effort towards the development of new polymeric formulations that would allow applying this technique to various fields of application, ranging from materials science to tissue engineering. However, most of the available materials are nevertheless oil-based and cost-ineffective. This work presents a novel bio-based resin for stereolithographic DLP 3D printing formulated by mixing a photocurable polyester obtained from renewable resources (poly(1,3-propanediyl-*co*-glyceryl) itaconate-*co*-vanillate, PPGIV) with methacrylated citrate and itaconate crosslinkers (bis(HEMA) itaconate, BHI, and tris(HEMA) citrate, THC) and appropriate photopolymerization initiators, terminators and dyes. As a proof-of-concept, a photocurable ink is formulated with phosphorescent Ir(III) cyclometalated complexes and its potential applications have been demonstrated for both rigid and flexible structures.

Introduction

Additive manufacturing (AM), or three-dimensional (3D) printing, is a computer-aided production technique that translates virtual 3D models into customized products of desired shape, design and size. The basic principle of additive manufacturing is building up an object layer by layer; in the first stage the design of the desired object is created by Computer Aided Design (CAD) and the virtual model is then digitally sliced into horizontal layers for a printable command sequence. *Via* a command file, the virtual coordinates are sent to a 3D printer, which deposits the material in predesigned locations at the *x*–*y* plane and the entire process is repeated along the *z* axis. Compared to traditional manufacturing techniques, modifications in the shape of the 3D printed manufacts can be easily performed by modifying the digital object, without the need for unique tools for a single modification.[1] Furthermore, 3D printing is a sustainable manufacturing process, as additive fabrication results in much less material waste.[2]

Amongst the various techniques that can be employed for the construction of 3D objects, stereolithography (SLA) plays a major role, as it allows building structures by selectively photocuring layer-by-layer a well formulated monomeric liquid ink. Commercially available inks for SLA can either be composed of acrylate- or epoxy-based mixtures. The most common approach is the employment of acrylate or methacrylate monomers or polymers, such as poly(ethylene glycol) diacrylate, poly(propylene glycol) diacrylate, bisphenol-A dimethacrylate, methacrylic acid and methacrylated aliphatic diols, together with pentaerythritol tetraacrylate as a crosslinker.[3–6] However, the hardening of the resin is sometimes performed exploiting the ionic chain polymerization of epoxides, such as 3,4-epoxy cyclo-methyl-3,4-epoxy cyclohexane carboxylate, with branched diols like 1,4-butanediol diglycidyl ether.[7,8] Novel and most promising materials for SLA 3D printing allow for the production of 3D printed polymers with a shape-memory effect,[9] stimuli-responsive materials,[10] stretchable hydrogels[11] and elastomers[12] for applications ranging from tissue engineering to materials science.[13,14] In addition, functional components are sometimes added to the inks, like organic fluorophores or conductive nanostructures.[15–17]

Amongst other applications, 3D printing technology is taking space in the textile/fashion industry due its ability to directly produce clothing from 3D printable raw materials in a single manufacturing operation. The application of AM to the textile industry is currently driven by the possibility to easily personalize clothing and to reduce the manufacturing costs, together with the possible implementation of a wide spectrum of new materials that could not find a place in traditional textile manufacturing.[18] AM techniques such as SLS[19] and FDM[20,21] have been widely explored for applications in this field. Surprisingly, very little effort has been yet directed towards the employment of photocured materials (SLA/DLP) for textile applications. This is probably due to the main challenge among the different mechanical properties needed, the

Department of Industrial Chemistry "Toso Montanari", University of Bologna, Viale Risorgimento 4, 40136 Bologna, Italy. E-mail: mauro.comesfranchini@unibo.it

†Electronic supplementary information (ESI) available. See DOI: 10.1039/d0gc01983f

elongation at break which has to be high but maintaining good mechanical resistance and lower fragility. Thanks to the possible organic manipulation of suitable building blocks from natural sources we believe that this technique might be a future system for the green fashion industry.

In general, most of the developed formulations for SLA/DLP are still derived from non-renewable resources, and often cost-ineffective.[22] Only a few examples of publications in the recent literature with strong effort toward the implementation of biomasses in stereolithography can be found, but the biomass loading into these resins still remains very low (<15%).[23–25]

Therefore, there is a need for the implementation of bio-based compounds into the formulations for 3D printing to the final consumer. This would allow the overall reduction of the carbon footprint of 3D printing technologies as a green and sustainable approach to rapid prototyping. The most promising bio-derived photocurable monomer is indeed itaconic acid, obtained by distillation of citric acid or by direct fermentation of glucose by specifically engineered bacterial strains.[26–28] It is able to undergo slower photopolymerization compared to acrylates and methacrylates due to its more hindered unsaturation, but its polyesters have been widely explored as a novel class of photocurable bio-based polymers.[29,30] Interestingly, a cyclodextrin derivative of itaconic acid (cyclodextrin itaconate) is used for the modification of cotton fabric, a market expected to raise remarkably.[31] Indeed, the impressive progress in the textile industry, with enormous production of cotton, is designed to be increasingly open to the itaconic acid market.

Herein, we present the development of a fully bio-based resin for DLP 3D printing for applications in rapid prototyping and modelling, and thanks to its mechanical properties a potential outlet in the textile/fashion industry has opened. So far, no successful attempt in developing such a total bio-based resin has ever been reported. To improve printing resolution, we also describe a series of crosslinkers able to make objects in reasonable time-scales without diffusion of the polymerization front outside the irradiated regions and with acceptable light penetration. We show here a total bio-based content of the novel ink as high as 96.5%, as far as we know this is the highest percentage ever reached. To achieve the desired final mechanical performance, *i.e.* high elongation at break, the suitable combination of itaconic acid and the two polyols has been deeply investigated. Therefore, mechanical performances of the 3D printed objects are evaluated in light of potential applications as both rigid and flexible structures,[32] the latter being potentially suitable in the textile industry.

The resin is formulated with different dyes and phosphorescent Ir(III) complexes as an additional proof-of-concept. We approached the addition of phosphorescent iridium complexes in order to demonstrate the versatility of the resin, the photostability of said complexes to prolonged irradiation during 3D printing and their effectiveness at very low concentrations. To the best of our knowledge this has never been demonstrated in the literature. The only implementation of transition metal complexes in stereolithography 3D printing techniques in the literature is the one reported by Lim *et al.*, in which they employed tris-bipyridyl ruthenium as the photoinitiator, but no photoluminescence property was discussed.[33]

Experimental section

All chemicals were purchased from Sigma-Aldrich Co. (St Louis, MO, USA) and used as received.

Synthetic procedures

Synthesis of the polyester – poly(1,3-propanediyl-*co*-glyceryl) itaconate-*co*-vanillate (PPGIV). The polyester resin has been synthesized by neat thermal polycondensation, similarly to what was previously described by Barrett *et al.*[30] In an amber round-bottomed flask, itaconic acid (1 mol, 130.1 g), glycerol (0.5 mol, 46 g), 1,3-propanediol (0.5 mol, 38 g) and vanillic acid (0.22 mol, 37 g) were stirred at 145 °C under nitrogen flux. After a homogeneous melt formed, the mixture was stirred for two hours under nitrogen flow. The pressure was then reduced to approximately 20 Torr and the mixture continued stirring for at least 5 hours. After cooling, the crude product was dissolved in chloroform (250 mL) or ethyl acetate (200 mL) and purified by filtration of the insoluble unreacted vanillic acid. The solvent solution was then washed several times with a 10% $NaHCO_3$ aqueous solution, water and brine. An oily brown product (76 g) was then obtained after drying the organic phase over anhydrous Na_2SO_4 and evaporating the solvent under vacuum. After the synthesis, the polyester was stored at room temperature in chloroform solution (around 50 wt%) to avoid polymerization to occur. Alternatively, the polymer can be stored in ethanol with the presence of 1–2% chloroform as a stabilizer. Yield = 34.8%, calculated as the ratio between the obtained mass of polymer and the sum of the masses of the employed reagents minus the amount of water condensed away after applying the vacuum to the reaction flask (32.8 g).

Synthesis of bis(2-(methacryloyloxyethyl) itaconate (BHI). In a round-bottomed flask, 300 μl of H_2SO_4 were added to a stirred dispersion of 130.1 g of itaconic acid (IA, 1 mol) and 194 mL of 2-hydroxyethyl methacrylate (HEMA, 1.6 mol) in 1 L of toluene. Alternatively, 2-methyl THF (1 L) or methyl cyclopentyl ether (1 L) can be used without significantly affecting the resulting product and yield.

The reaction was allowed to occur for 72 h at 70 °C. The solvent was then evaporated to obtain a yellow liquid which was then dissolved in the minimum amount of ethyl acetate. The organic phase was washed three times with a saturated $NaHCO_3$ solution to remove unreacted itaconates and then dried over anhydrous Na_2SO_4, and filtered and the solvent was evaporated to obtain the product as a pale-yellow liquid. Yield = 77%. ^{1}H NMR (DMSO-d_6, 400 MHz, δ): 6.10–5.98 (m, 3H), 5.70–5.60 (m, 3H), 4.36 (s, 1H), 4.28 (s, 1H), 4.12 (m, 4H), 3.62 (m, 4H), 1.89 (m, 6H), Fig. S3.† ESI-MS: 377 [M + Na^+].

Synthesis of tris(2-(methacryloyloxyethyl) citrate (THC). In a round-bottomed flask, 380 μl of H_2SO_4 were added to a stirred

dispersion of 160 g of citric acid (CA, 0.83 mol) and 300 mL of 2-hydroxyethyl methacrylate (HEMA, 2.5 mol) in 1.3 L of toluene. The reaction was allowed to occur for 24 h at 70 °C. The solvent was then evaporated to obtain a yellow liquid which was then dissolved in a minimum amount of ethyl acetate. The organic phase was washed three times with a saturated $NaHCO_3$ solution to remove unreacted citrates and HEMA, and then dried over anhydrous $NaSO_4$, filtered and the solvent evaporated to get the product as a pale-yellow liquid. Yield = 81%. ^{1}H NMR ($CDCl_3$, 400 MHz, δ): 6.12 (m, 3H), 5.57 (m, 3H), 4.25 (m, 6H), 3.83 (m, 6H), 2.43 (m, 4H), 1.93 (m, 9H), Fig. S4.† ESI-MS: 551 [M + Na^+]. Other solvents such as 2-methyl THF (1.3 L) or methyl cyclopentyl ether (1.3 L) can be used to replace toluene, without significantly affecting the resulting product and yield.

Synthesis of the phosphorescent Ir(III) complexes. The cationic [Ir(ppy)$_2$(bpy)]Cl complex has been synthesized as reported in the literature,[34] while the anionic Ir(III) complexes have been synthesized according to the procedure developed by some of us in 2017.[35]

Resin formulation

The photocurable ink was prepared by placing in a round-bottomed flask a certain amount of PPGIV solution in chloroform, after which the solvent is removed firstly by rotary evaporation and then with high vacuum. The polyester mass was weighed and the other components were added in their predetermined relative proportions. Photopolymerization initiators and terminators were added as pure solids, while THC and BHI were added as purified liquids. Organic dyes and Ir(III) complexes were added from 1 mg mL^{-1} stock solutions in chloroform or methanol, depending on their solubility. Then, around 20% of solvent (out of the total ink weight) is added and the mixture is magnetically stirred for 30 min to ensure the homogeneous mixing of all components; chloroform ethanol, methanol and ethyl acetate all work well. Finally, the organic solvent is mostly removed by rotary evaporation and then by applying high vacuum until no bubbling was observed.

DLP 3D printing

Dog-bones for tensile and flexural tests have been drawn by computer-assisted design (CAD), the former matching the ISO-527-1BA specifications, while the latter was a simple 80 × 10 × 4 mm rectangular bar; otherwise, small dog-bones and a bigger representative model have been downloaded from an open-source website (Fig. S5†).[36] Afterwards, the 3D digital models have been sliced with Creation Workshop (V2.3) software, provided by the printers manufacturers. A Sharebot Sprit DLP 3D printer has been employed for the 3D printing of all the models; it is equipped with a white-light DLP projector (3000 ANSI Lumen) capable of 1920 × 1080 pixel resolution, related to a x–y nominal printing resolution of 50 μm. The total printing area is 54 × 96 × 100 mm, and it allows vertical printing speeds up to 4 cm h^{-1} with tuneable z resolution up to 20 μm. For the developed resin, irradiation time and platform movement parameters have been optimized to increase the printing speed while still achieving good printing resolution and structural stability. In general, the developed resins allowed for efficient printing with exposure times between 3 and 5 s per layer. Dog-bones for tensile tests and bars for flexural tests have been printed with a 15° angle between their normal and the building platform, to reduce the formation of cracks during the detachment of the printed layers from the resin tank. Since the total printing time mostly depends on the number of layers to be printed, it could vary between 2 and 16 h depending on the height of the specimen to be printed and the desired z resolution. For each printed model, the required printing time is shown in Fig. S5.† After the printing process, the photocured resins have been detached from the printing platform and soaked in 2-propanol for 15 min in order to allow for the unreacted resin to be washed away. Then, the raw 3D printed objects are allowed to cure and dry for one week by exposing to air and environmental light.

Characterization

^{1}H and ^{13}C NMR spectra were obtained on Varian Inova (14.09 T, 600 MHz) and Varian Mercury (9.39 T, 400 MHz) NMR spectrometers. In all recorded spectra, chemical shifts have been reported in ppm of frequency relative to the residual solvent signals for both nuclei (^{1}H: 7.26 ppm for $CDCl_3$ and 2.50 ppm for DMSO-d_6. ^{13}C: 39.52 ppm for DMSO-d_6). ^{13}C NMR analysis was performed using ^{1}H broad band decoupling mode. Solvent-suppressed ^{1}H NMR spectra have been recorded with pre-saturation pulse sequences. Mass spectra of the cross-linkers were recorded on a micromass LCT spectrometer using electrospray (ES) ionisation techniques.

Size exclusion chromatography (SEC)/gel permeation chromatography (GPC) was performed on a Shimadzu CBM-20A system (controlling a LC-10AD pump equipped with a DGU-20A degasser, a SIL-20A autosampler and a RID-20A refractive index detector). A TSKgel G5000HHR column (5 μm particle size 0.78 cm × 30 cm) and a TSKgel HHR-H Guard (5 μm particle size 6.0 × 40 mm) guard column were used as column systems. The measurements were performed at 40 °C to ensure the reproducibility of the measurements. HPLC grade chloroform was used as the eluent with a flow rate of 1 min mL^{-1}. The system was calibrated with PS standards obtained from PSS covering a molar mass range from 370–2 520 000 g mol^{-1} (ReadyCal-Kit Polystyrene). Polymer solutions with a concentration of 3 mg mL^{-1} were prepared by dissolving 15 mg of polymer in 5 mL HPLC grade chloroform. Subsequently, the samples were sonicated for approx. 10 min at 55 °C. Prior to injection, the samples were filtered with a 0.45 μm PTFE and a 0.2 μm PTFE syringe filter to remove eventually occurring insoluble impurities (*e.g.*, dust). An injection volume of 50 μL was chosen for the measurements and a measurement time of 30 min was applied to avoid overlapping of eventually occurring solvent signals in the subsequent measurements.

Differential Scanning Calorimetry (DSC) has been performed with a Mettler Toledo DSC 3+ Star system heating the sample from −50 °C to +200 °C with 10 °C min^{-1} heating rate and 50 mL min^{-1} N_2 flow. For thermogravimetric analysis

(TGA), a Mettler Toledo TGA 2 Star system has been employed. The sample has been heated from 25 °C to 600 °C with a heating rate of 10 °C min^{-1} and 50 mL min^{-1} N_2 flow.

Rheological measurements were performed using a rheometer (Malvern Kinexus Pro+) equipped with CP1/60: PL65 geometry, meaning a 60 mm diameter with 1° angle cone over a 65 mm plate. The temperature of the plate was varied over the 15 °C–35 °C temperature range. Ink viscosities were measured *via* a logarithmic sweep of shear rates ranging from 1 to 100 Hz. Oscillatory experiments were performed at a constant frequency of 1 Hz.

For a tensile test and a flexural test, a Zwick/Roell Z010 machine was employed with a test speed of 1 mm min^{-1} (ISO527-1BA) and 2 mm min^{-1} (ISO178) for tensile and flexural tests, respectively. A maximum stress of 10 kN was applied. Impact strength was determined with CEAST 9050 impact pendulum with a Charpy configuration, impact energy of 1 J at a temperature of 23 °C (ISO 179-1eU). Hardness has been evaluated with a Shore D tester TH210 (Time Group Inc.) following ISO868 specifications.

Photophysical studies on phosphorescent 3D printed materials have been performed with an Edinburgh FLSP920 spectrofluorometer equipped with a 450 W Xenon arc lamp. ATR-FTIR analysis has been performed using a Cary 630 FTIR spectrometer (Agilent). SEM images were acquired with a field emission gun scanning transmission electron microscope ZEISS LEO Gemini 1530 (FEG-STEM).

In vitro biocompatibility tests

Human keratinocytes (HaCaT) have been used for performing *in vitro* biocompatibility tests; cells were maintained in Dulbecco's modified Eagle's medium (DMEM) (Euroclone, Milan, Italy) supplemented with 10% fetal bovine serum (FBS), 1% penicillin–streptomycin, and 1% glutamine (Lonza, Basel, Switzerland). Printed samples have been rinsed with DMEM and the eluate has been collected: cells were seeded on polystyrene multiwell culture plates (12 wells) with a cell density of 20 000 cells per well. A DMEM-eluate volume was added to treated samples as normal medium, control samples were treated with bare DMEM, finally cells were incubated at 37 °C, 5% CO_2 overnight. Optical microscope observation and cell counting have been performed.

Preliminary evaluation of cytotoxicity (MTT assay) and evaluation of pro-sensitizing activity (FACS analysis) on human monocytes (THP-1) have been performed following the normative reference OECD Guideline 442E, Annex 1 "*In vitro* Skin Sensitization; Human Cell Line Activation Test (hCLAT)". Monocyte-like human cells THP-1 were kept in RPMI medium containing 10% FCS and 2 mM glutamine. The sample has been eluted in PBS for 24 hours at 37 °C. The eluted sample was diluted in the cell culture medium, and the cell medium exposed to the same experimental conditions was used as a negative control. The exposure has been carried out for 24 h at 37 °C with 5% CO2. After the incubation, cells are collected, checked under the microscope for their viability by staining with Trypan Blue dye and counting in a cell counter chamber, washed in PBS and then marked with a fluorescent anti-Intercellular Adhesion Molecule (CD54) or B7.2 (CD86) antibody and in both cases with a propidium iodide (PI) solution to simultaneously measure the percentage of dead cells. Only viable cells are included for analyses of CD54 or CD86 expression. After washing, to eliminate the excess antibody, the MFI (Mean Fluorescence Intensity) linked to the cells is evaluated by means of a flux cytofluorimeter (FACS, Fluorescence Activated Cell Sorter, Becton Dickinson, Mountain View, CA). This value is proportional to the expression of co-stimulatory molecules. The results are expressed in terms of MFI (Mean Fluorescence Intensity).

As acceptance criteria, the percent of living cells (PI negative) must be above 80% in all samples. The MFI of the positive control must be >10% of the negative control at the lowest tested concentration of nickel (Table S2†). The MFI must display a dose–response increasing pattern with the other two tested doses.

Results and discussion

Photocurable polyester, poly(1,3-propanediyl-*co*-glyceryl) itaconate-*co*-vanillate (PPGIV)

Since itaconic acid is a water-soluble solid diacid, its derivatization is definitely required in order to obtain a liquid 3D-printable resin. Based on a previous study by Barrett *et al.*,[30] itaconic acid was reacted with different alcohols at high temperatures under vacuum to obtain photocurable liquid polyesters that, being the main component of the developed ink, could be formulated for the desired application. For the preparation of the optimum liquid polyester, polycondensation under vacuum without solvent was employed: several different bio-based hydroxy derivatives such as alcohols, diols, polyols, and hydroxy acids have been tested, alone or in mixtures, but eventually most of them have been discarded either for their low printability, their high cost or the worse performances of their poly-itaconates (Table S1†). Finally, the bio-based monomers which allowed the formation of itaconic acid polyesters with acceptable mass yield (35%), easy purification and DLP printability were glycerol, 1,3-propanediol and vanillic acid (Fig. 1) in 0.5 : 0.5 : 0.22 mixture compared to itaconic acid, respectively. 1,3-Propanediol is industrially manufactured by DuPont by fermentation of corn syrup and glycerol is the main waste material in the production of biodiesel. In addition, vanillic acid can be obtained by oxidation of vanillin, but it is also naturally occurring.[37–40]

The key component that allowed the preparation of a fully printable ink for DLP 3D printing was indeed vanillic acid (Fig. S17†). Even though, being a hydroxy-acid, it does not compete with the other components during the formation of the polyester, it played a fundamental role in the light-absorption processes taking place during the photopolymerization. In fact, most of the time, in photopolymerization-based 3D printing techniques the addition of photoabsorbers such as 2,5-bis(5-*tert*-butyl-benzoxazol-2-yl)thiophene (BBOT) or dyes is

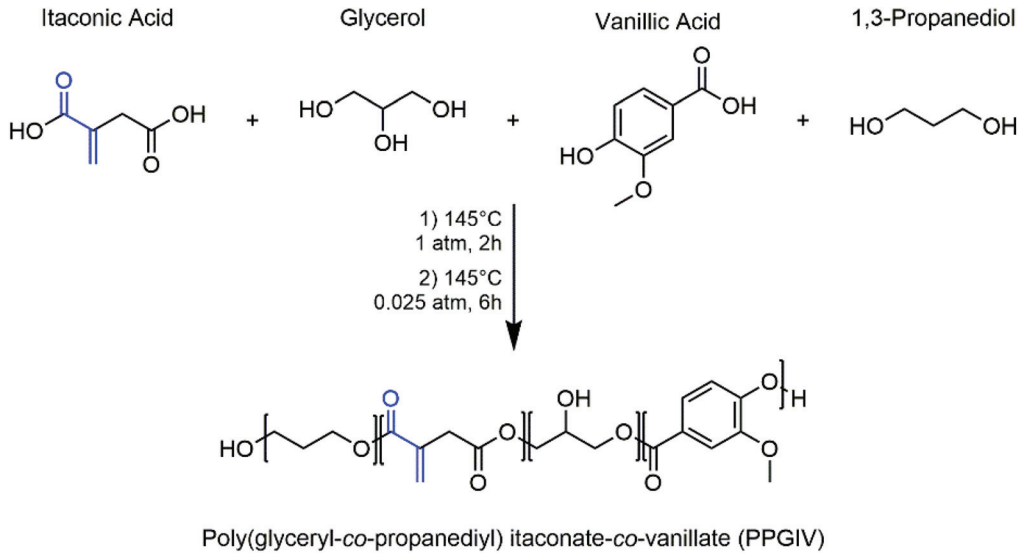

Fig. 1 Selected monomers and experimental conditions for the preparation of the photocurable polyester. The photopolymerizable group of itaconic acid is highlighted in blue.

essential.[41] This is because it is often required to limit the diffusion of high-energy photons into the resin during the photopolymerization process, to avoid diffusion of the polymerization front outside the irradiated section which can cause a drastic reduction in the *x*–*y* resolution of the printed object. In our case, the task is performed by a combination of the effect of the vanillic acid monomers contained in the polyester chains and the dyes added to the formulation. Less remarkably, the incorporation of vanillic acid into the resin gives it a pleasant sweet vanilla flavour, as opposed to commercial resin which displays the unpleasant characteristic smell of acrylate compounds.

The synthesized itaconic acid-based photocurable polyester poly(1,3-propanediyl-*co*-glyceryl) itaconate-*co*-vanillate (PPGIV) was characterized by NMR spectroscopy (^{1}H-, ^{13}C-, qHSQC and qHMBC), to evaluate its purity and the effective incorporation of all the selected components (Fig. 2, S1 and S2†). NMR analysis reveals the presence of peaks related to each of the employed monomers, but no unreacted reagents are present.

The application of ^{13}C NMR to determine whether the glycerol units lead to branched structures by reaction of their secondary alcohol moiety has been previously described by Somisetti *et al.*[42] In their work, the authors related the middle carbon in glycerol units to a ^{13}C NMR peak around 69 ppm for branched glycerol units and a peak around 65 ppm for linear or terminal ones. In our case, we observe peaks in both regions, suggesting the coexistence of terminal, linear and branched glycerol units in the synthesized polyester. This is also confirmed by the qHSQC and qHMBC spectra of PPGIV reported in Fig. S2.†

The weight and molar compositions of the obtained polymeric resin were evaluated on a fully hydrolysed polyester sample by NMR spectroscopy. Results are reported in Table 1, and the whole calculation is available in the ESI.† Strongly alkaline conditions such as NaOH 3 M in deionized water and high working temperatures (around 80 °C) allowed for the complete saponification of the polyester resin, generating much simpler NMR spectra which display the signals for each employed monomer (Fig. S6†).

The average molecular weight of the polyester was determined by size exclusion chromatography (SEC)/gel permeation chromatography (GPC), revealing that for the prepared polymer M_n = 1500 g mol^{-1} and M_w = 1650 g mol^{-1}, corresponding to PDI = 1.1. A low polymerization degree is expected for catalyst-free thermal polycondensations, and it is required for the obtainment of relatively low viscosity liquid solutions that could be efficiently formulated into liquid resins for 3D printing.

Crosslinkers

Even though PPGIV is rich in itaconic acid, and thus in photocurable double bonds, their concentration is too low for applications in DLP. The photopolymerization of the polyester itself leads to a cured polymer which does not display the mechanical performances required for it to keep its shape during the 3D printing process, causing the structure collapse under its own weight. Moreover, even at low molecular weights the viscosity remains too high, preventing its diffusion onto the resin vessel between the curing of one layer and the next during the 3D printing process, making it extremely hard to employ it as-it-is for the final application. In order to overcome both these problems, the new compounds bis(HEMA)itaconate (BHI) and tris(HEMA) citrate (THC) crosslinkers have been synthesized by adapting a procedure available in the literature for the formation of the bis(isopropyl) ester of itaconic acid (Fig. 3).[43]

The required chemicals are cheap, and the reactions allow producing large amounts of crosslinkers (yields for BHI of 77% and for THC of 81%) with high purity and little efforts for

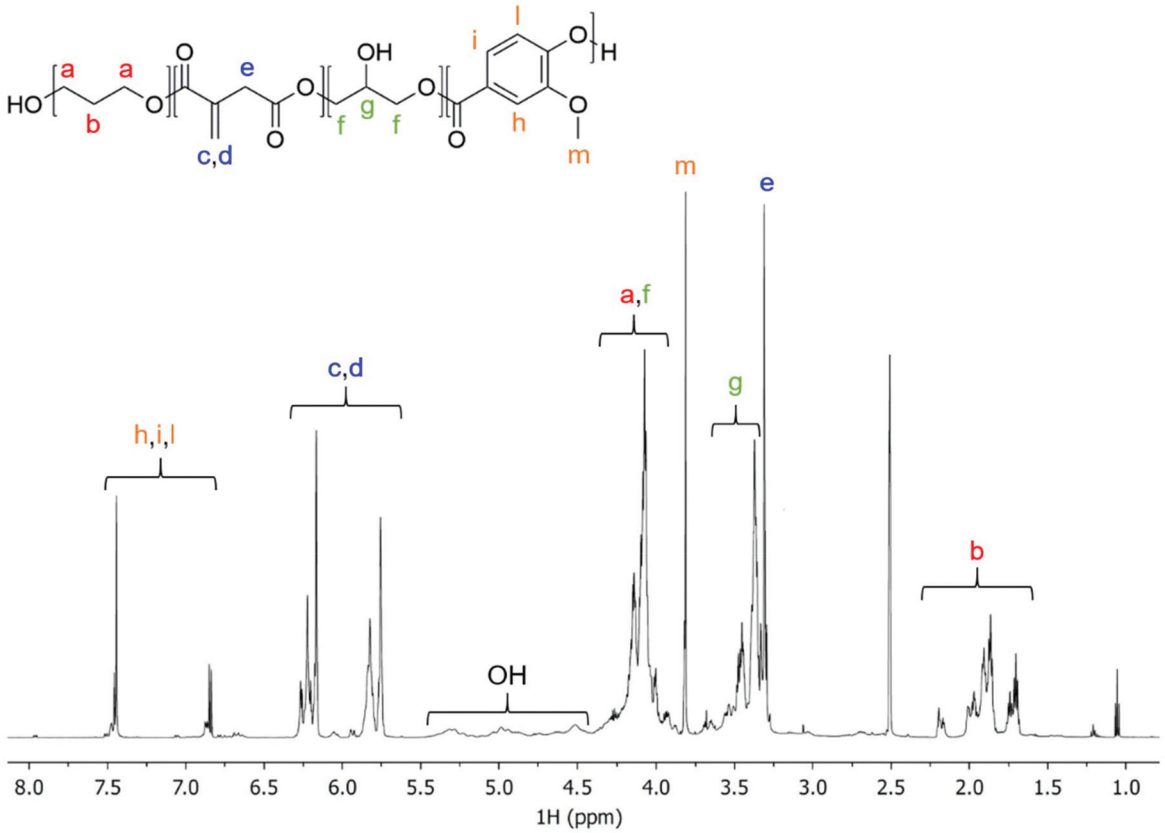

Fig. 2 ^{1}H NMR spectrum (600 MHz, DMSO-d6) of PPGIV, with the assignment of peaks to the related monomers or functional groups.

Table 1 Monomer composition of the synthesized PPGIV and the corresponding minimum molecular structure representing the proportions between the monomers

Component	Molar ratios	Weight percentage
Itaconic acid	6.5	51%
1,3-Propanediol	4.7	22%
Glycerol	3.0	17%
Vanillic acid	1.0	10%

their purification. Notably, the two compounds are both liquids with low viscosity and low volatility; they are totally bio-based and display high density of photocurable groups. In addition, the use of 2-hydroxyethyl methacrylate (HEMA) for the preparation of the crosslinkers is preferred, due to its low toxicity and low volatility compared to other acrylate compounds,[44,45] and the biocompatibility and biodegradability of many polyHEMA copolymers have been well established

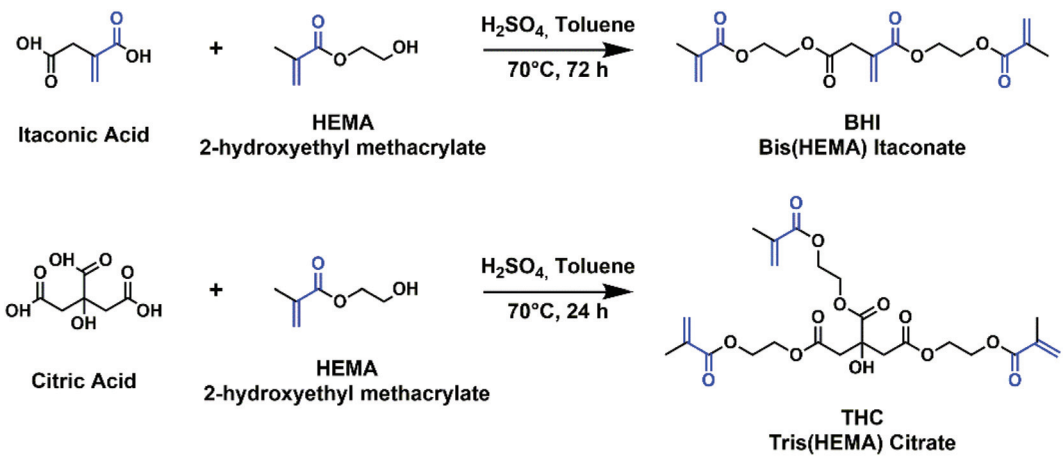

Fig. 3 Chemical reactions for the synthesis of the crosslinkers. The photocurable acrylate moieties are highlighted in blue.

in the literature.[46–48] Furthermore, HEMA can be obtained *via* renewable oil-free processes, as it is often produced by esterification of methacrylic acid with ethylene glycol: the former can be produced by catalytic oxidative dehydrogenation of bio-synthesised isobutyric acid, and the latter can be obtained by fermentation of D-xylose in engineered *E. coli*.[49–53]

The employment of different acrylate crosslinkers for DLP 3D printing such as isobornyl acrylate, pentaerythritol tetraacrylate and multifunctional acrylate oligomers was previously reported, but these derivatives suffer from several drawbacks such as high cost, low bio-content and the required employment of toxic acrylates during their production.[54]

Ink formulation

Besides the photopolymerizable substrate, the main components required for the 3D printing are: (i) photopolymerization initiators, (ii) photopolymerization inhibitor, (iii) crosslinkers and (iv) dyes (Fig. 4). As initiators, we observed that the fastest curing is achieved with the combination of two acylphosphine oxides (phenylbis(2,4,6-trimethylbenzoyl)phosphine oxide, BAPO and diphenyl(2,4,6-trimethylbenzoyl)phosphine oxide, MAPO) together with 2,2-diethoxy acetophenone (DEAPH). The initiators are required to efficiently absorb the UV light generating reactive radicals that can propagate in the ink leading to the polymerization of the double bonds. As a terminator, 4-methoxyphenol (MHQ) has been selected as it is relatively safe, low cost and very effective.[55]

The crosslinkers have already been discussed in the previous paragraph. As aforementioned, dyes participate together with vanillic acid residues in the absorption of UV light diffusing into the resin outside of the irradiated regions, allowing for better printing resolution.[56]

In order to demonstrate the great versatility of the final formulation, we explored four organic dyes to cover the full visible spectrum of colours: methyl red (red), cresol red (yellow), solvent green 3 (1,4-bis(*p*-tolylamino) anthraquinone, green) and unisol blue AS (1,4-bis(*p*-isopropylamino) anthraquinone, blue) (Fig. 4).

The red and yellow dyes are commonly employed acid–base indicators: since the prepolymer displays free carboxylic groups from terminal itaconic acid monomers, they display their acid colour when formulated into the ink. The green and blue dyes, instead, are anthraquinone derivatives, which can be employed in ppm concentrations thanks to their extensive molar absorption coefficients. The ink was then formulated by mixing all the required components in pre-defined ratios with organic solvents such as ethanol, methanol, ethyl acetate or chloroform at room temperature. The evaporation of the solvent, firstly by rotary evaporation and then by applying high vacuum, allowed for the obtainment of a homogeneous photocurable ink ready to be subjected to the 3D printing process.

The optimal relative amount of the different components is reported in Fig. 5. To recap, the final formulation contained 48.5 wt% of PPGIV, 24.0 wt% of BHI and 24.0 wt% of THC, 1.5 wt% of initiators, 2.0 wt% of terminator and 0.01 wt% of dyes. Since the first three components can be considered as bio-based, the herein reported formulation has a nominal bio-based content of around 96.5%.

In order to avoid photopolymerization of the resin induced by environmental light, the developed resins have been stored at room temperature in amber glass containers. Under these conditions, the resin demonstrated stability and printability up to 12 months due to the presence of the inhibitor MHQ that would immediately quench any possible radical species spontaneously formed.

Rheological analysis has been performed on the formulated resin to determine its printability *via* DLP and stereolithographic technique. If the viscosity of the ink is too high, it will require longer printing times: it will be required to reduce the speed of the moving platform to allow the resin to fully flow underneath it, between the irradiation of one layer and the next. In addition, if the ink displays marked non-Newtonian shear thickening behaviour, it will react to the movement of the building platform inside it with a variation in its overall viscosity, again resulting in a need for a reduction of the platform movement speed. As shown in Fig. 6, the developed bio-based ink displayed viscosity in the 0.07–0.3 Pa s range, and a Newtonian behaviour is observed. Nevertheless, the measured viscosity in the range of operating temperatures (15–35 °C) would indeed allow for the resin to flow and fully cover the printer's resin vessel in the minimum timeframe of 3 s.

The fluid behaviour of the ink was also confirmed by oscillometric viscoelasticity studies as a function of temperature (Fig. 6). As the phase remained constant throughout all the temperature range around 90°, the ink mostly resembled the features of a liquid, as it is also observed by the low storage modulus. The developed formulation was able to undergo DLP 3D printing leading to the formation of well-resolved solid objects. Several irradiation times have been tested to minimize the printing time while still maintaining good resolution and structural stability. The identified optimal irradiation time was 3000 ms and accordingly, several test samples have been printed and underwent mechanical analysis to assess the mechanical properties of the formulated ink. In particular, flexural and tensile strength analysis, Charpy impact test and evaluation of shore-D hardness have been performed on 3D

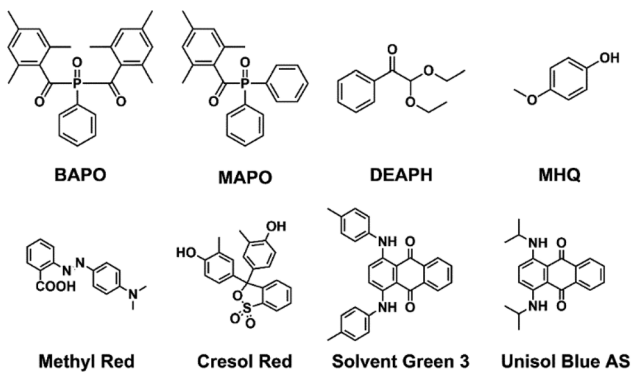

Fig. 4 Chemical structure of the selected photopolymerization initiators (MAPO, BAPO and DEAPH), terminator (MHQ) and dyes.

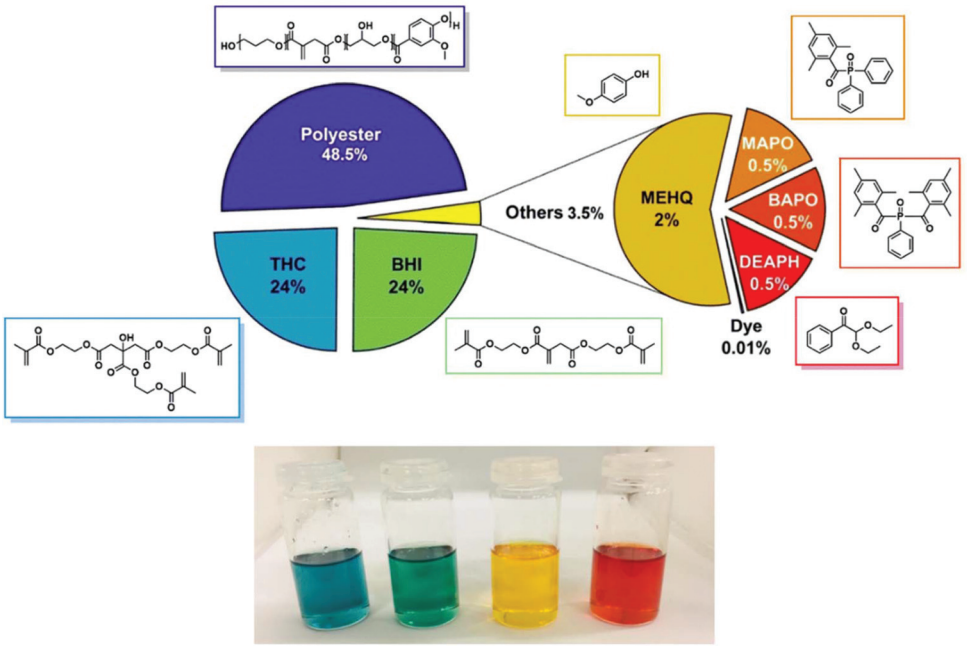

Fig. 5 Top: Weight composition of the developed bio-based ink for DLP 3D printing. Bottom: Optical picture of the developed resins with the four different dyes.

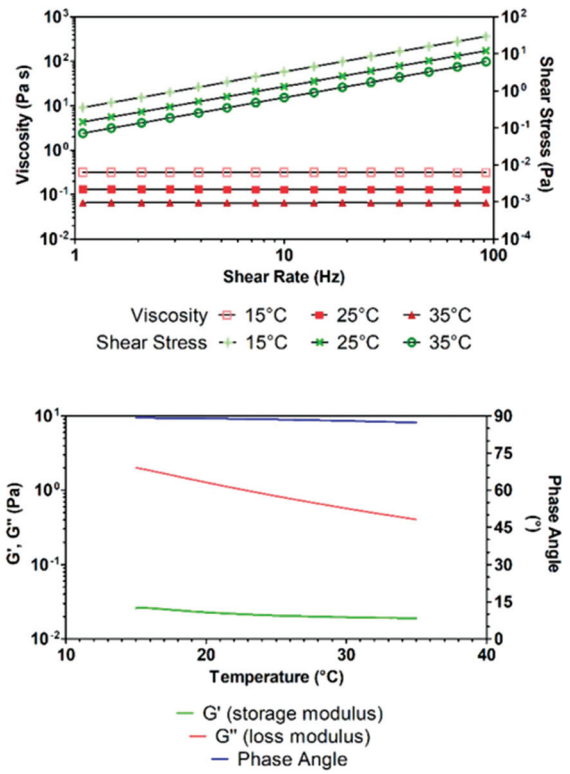

Fig. 6 Rheological analysis of the photocurable ink. Top: Shear stress and viscosity *vs.* shear rate relationships at different temperatures. Bottom: Temperature dependence of storage and loss moduli for the developed ink and the corresponding phase angle, obtained by oscillatory viscoelastic analysis.

printed specimens. The results of the mechanical tests are shown in Fig. S7 and S8† and summarized in Table 2. For tensile tests, dog-bones have been printed according to ISO-527-1BA specifications, while flexural tests have been performed on 80 × 10 × 4 mm rectangular bars.

3D printed objects

It is worth mentioning that the mechanical properties of layered objects printed by AM are intrinsically anisotropic, and the outcome of these tests is strongly dependent on the direction along which the mechanical stress is applied.[57] This makes it very trivial to evaluate mechanical performances of commercially available resin formulations if the printing geometry is not described or standardized. In our case, the tensile stress vector was tilted 15° with respect to the z printing direction, while the bending stress vectors were tilted 75° with respect to it (Fig. S7 and S8†).

First of all, we can notice good mechanical resistance and lower fragility which are the minimum requirements to get a printed object. For instance, the object made with the developed formulation displays four times greater impact strength (internal data on a commercial resin) with a value of 4.77 kJ m^{-2}. Moreover, the fabricated objects display good flexural properties, enabling bending deformations up to 6%, with flexural strengths around 12.6 MPa. The textile industry needs flexibility and indeed the first thing to be noticed is the low tensile modulus of our bio-based construct, revealing that the polyester-based ink displays increased elasticity. Compared to acrylate-based formulations, the presence of low molecular weight polyesters gives higher elasticity. This is also confirmed by its very high elongation at break up to 18%; in comparison

Table 2 Mechanical properties of 3D printed objects built with the developed ink

Tensile test			Hardness [Shore-D]	Impact strength [KJ m^{-2}]
E_t tensile modulus [MPa]	σ_{tb} ultimate tensile strength [MPa]	ε_{tb} elongation at break [%]		
62 ± 5	5.4 ± 0.7	18.0 ± 2.9	72 ± 1	4.77 ± 2.81

Flexural test				
E_f flexural modulus [MPa]	σ_{fm} maximum flexural strength [MPa]	ε_{fm} deformation at maximum strength [%]	σ_{fb} ultimate flexural strength [MPa]	ε_{fb} deformation at break [%]
350 ± 25	12.6 ± 1.8	5.4 ± 0.7	12.6 ± 1.8	5.4 ± 0.7

commercial resins give values in the range of 2–5%. The developed ink also displays low ultimate tensile strength: due to the fact that the tensile test has been performed in the direction perpendicular to the printed layers, it is reasonable to suppose that the lower value is due to a lower adhesion between the printed layers which, upon traction, detach from each other by weaker forces.

The effective polymerization of the mixture was confirmed by ATR-FTIR spectroscopy performed on the 3D printed objects compared to the uncured resin (Fig. S9†). The absorption at 1636 cm^{-1}, attributed to the stretching of the C=C group, and the ones at 944 and 815 cm^{-1}, related to C=C–H deformations, are strongly reduced in intensity, suggesting the effective formation of a network of saturated C–C bonds at the expense of itaconic and methacrylate groups.

Then, scanning electron microscopy (SEM) was employed to assess the actual printing resolution achievable with the developed resin (Fig. S10†), allowing not only the visualization of the juncture of the printed layers, but also the size of the actual pixel irradiated by the DLP projector, confirming the 50 × 50 μm *x*–*y* resolution declared by the printer manufacturers and the 50 μm layer thickness set in the slicing phase. It is also possible to notice the great homogeneity of the printed surface at the micron scale, with little or no fractures and well-defined edges and vertices.

Finally, thermal analyses (DSC and TGA) have been performed on the printed objects (Fig. S11 and S12†). DSC reveals the presence of one T_g for the polyester-based photocured material, which can be attributed to the glass-to-plastic transition of the polyester chains in the polyacrylate network. On the other hand, TGA reveals thermal decomposition of the printed objects starting at around 120 °C, with a first 50% mass loss below 400 °C. Compared to a commercial monomeric analogue, it degrades faster with increasing temperature, but it allows reaching comparable ash residue after calcination in air at 600 °C.

Phosphorescent inks

Undoubtedly, the textile/fashion industry is increasing its demands towards luminescent materials, as they are widely employed, for example, in safety clothing where the luminescence allows increasing the visibility of the wearer in dangerous environments. Moreover, in recent years luminescence of textiles has not been strictly employed as a purely functional attribute, but more and more to add a novel touch on basic design.[58] Currently, phosphorescent textiles are produced by deposition or chemical linking of phosphors to polymer fibres, which are then employed in the manufacturing of clothing.[59,60]

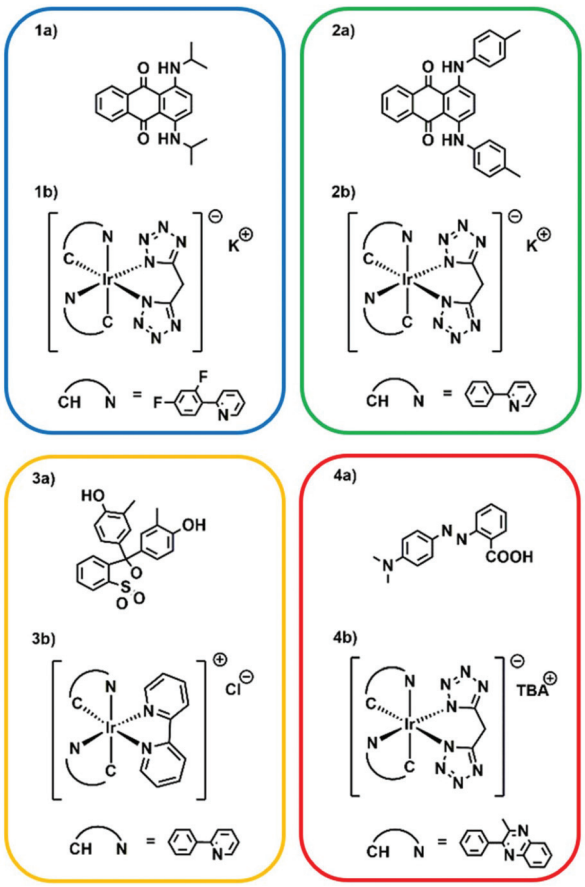

Fig. 7 Compatible dye-complex pairs selected for the formulation of the four phosphorescent resins. (1a) Unisol Blue AS and (1b) $[Ir(dfppy)_2(b\text{-}trz)]^-K^+$. (2a) Solvent Green 3 and (2b) $[Ir(ppy)_2(b\text{-}trz)]^-K^+$. (3a) Cresol Red and (3b) $[Ir(ppy)_2(bpy)]^+Cl^-$. (4a) Methyl Red and (4b) $[Ir(pqu)_2(b\text{-}trz)]^-TBA^+$Emission spectra of 3D printed luminescent dog-bones revealed that the emissive behaviour of the complexes has been maintained after the photopolymerization (Fig. 8a). Moreover, it was possible to notice with the naked eye the increase of emission intensity after the printing, induced by the molecular rigidity given by the liquid-to-solid transition of the polymer matrix in which the complexes have been dissolved.

Herein, as a proof-of-concept, four luminescent inks have been prepared by addition of phosphorescent iridium(III) cyclometalated complexes to the developed resin; this allowed the obtainment of inks capable of light emission throughout all the visible spectrum by excitation in the near UV range. The selected complexes are $[Ir(dfppy)_2(b\text{-}trz)]^-K^+$ as a blue emitter, $[Ir(ppy)_2(b\text{-}trz)]^-K^+$ as a green emitter, $[Ir(ppy)_2(bpy)]^+Cl^-$ as a yellow emitter and $[Ir(pqu)_2(b\text{-}trz)]^-TBA^+$ as a red emitter.[34,35] Considering that the dyes added to the formulation can absorb the light produced by the above-listed phosphors, a proper selection of suitable complex-dye pairs (Fig. 7) which displayed compatible emission and absorption behaviours was found to be fundamental; *i.e.* the dye should absorb in a region different from the emission region of the complex in order to avoid auto-absorption. It should be mentioned that cyclometalated Ir(III) complexes have been previously employed to generate reactive radical species upon light irradiation.[61–63] Therefore, we explored the possibility of employing the luminescent additives as photopolymerization initiators, but no hardening of the resin was observed for concentrations up to 0.5 wt% and irradiation times up to 10 s. Emission spectra of 3D printed luminescent dog-bones revealed that the emissive behaviour of the complexes has been maintained after the photopolymerization (Fig. 8a). Moreover, it was possible to notice with the naked eye the increase of emission intensity after the printing, induced by the molecular rigidity given by the liquid-to-solid transition of the polymer matrix in which the complexes have been dissolved.

Three-dimensional emission maps are shown in Fig. S13–S16.† Good emission intensities have been obtained with complex concentrations as low as 0.05 wt% for blue, green and yellow complexes, while it required 0.15 wt% of the red complex to give a noticeable emission, owing to the avowed lower phosphorescence quantum yield of the red complex.[35]

Very interestingly, reversible flexibility of the printed objects is clear from Fig. 8d and this confirms the very high elongation at break obtained and finally, in order to prove the overall performances of the developed ink in terms of printability and resolution, a bigger model was printed. The selected model represents the historical towers "Le Due Torri" from the city of Bologna, Italy (Fig. 8e). The selected ink contained the green complex–dye pairs and allowed for the reproduction of high-resolution details in the overall construction.

In vitro biocompatibility tests

Since a possible future target is the use of our resin in textile applications, an *in vitro* analysis of the pro-sensitising potential was carried out. For assessing the biocompatibility of our printed samples and with the aim of demonstrating that there is no intrinsic cytotoxicity, we carried out two different tests: a

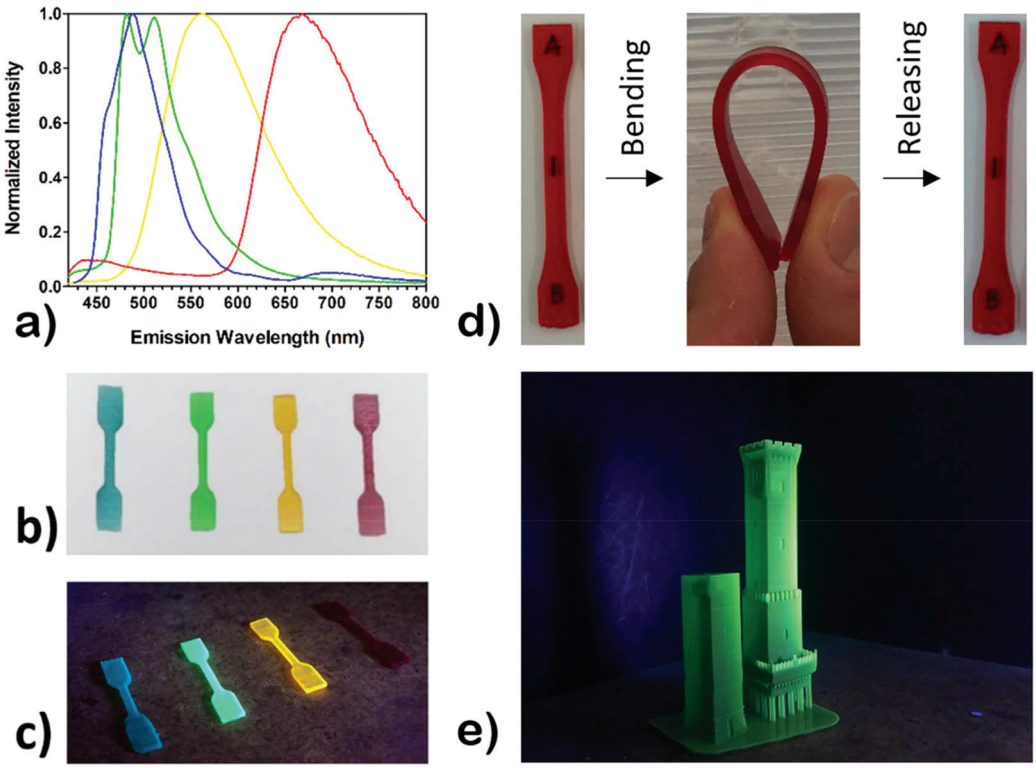

Fig. 8 DLP 3D printing of flexible and phosphorescent resins. (a) Normalized emission profiles of the iridium-containing 3D printed dog-bones. Each curve colour corresponds to the emission colour of the corresponding Ir(III) complex. The excitation wavelength is 360 nm for all emission spectra. (b) Optical camera pictures of the phosphorescent dog-bones exposed to visible and (c) UV (365 nm) light. Dog-bone dimensions are 6 × 1.8 × 35 mm. (d) Demonstration of the reversible flexibility of the printed objects. Dog-bone dimensions are 77 × 10 × 2 mm. (e) Picture of a 3D printed green phosphorescent model of "Le Due Torri" of the city of Bologna, under UV irradiation. Structure dimensions are 56 × 40 × 96 mm.

human keratinocyte viability test and an evaluation of pro-sensitising activity (according to OECD 442E) on human monocytes through FACS analysis.

Human keratinocytes seeded on polystyrene Petri dishes and exposed for 24 h to the sample eluate did not display any difference in terms of morphology, adhesion and proliferation. Optical microscopy observation and cell counting demonstrated that HaCaT cells can adhere and proliferate in the presence of sample's eluate (Fig. S18†).

For what concerns the pro-sensitising activity, the purpose of the test was to assess the absence of pro-sensitising skin effects from finished products or raw materials intended for contact with the skin or mucous membranes. In the assay, human monocytes cell line (THP-1) as a prototypic blood-derived immunologically active cell was used. On these cells, the expression of two costimulatory molecules, CD54 (Intercellular Adhesion Molecule) and CD86 (B7.2), was tested, using as a positive control Nickel sulphate, a well-known contact sensitising agent. Nickel sulphate is able to cause *in vivo* allergic immune reactions (skin sensitization) and it is also widely used to study *in vitro* immune response modulation. The increasing expression level of CD54 and CD86 on monocytes is a signal of activation of the immune response derived from the exposition to a potentially sensitising contact antigen.

The expression of co-stimulatory molecules on the dendritic cells means activation of the immunological response in terms of capability to present the antigen in the typical tissues (skin in this case), where, *in vivo*, the immune protective response is triggered. The costimulatory molecule expression is compared to the behaviour of nickel characterised by (a) high increase of both the markers; (b) direct correlation between concentration and intensity of the response; (c) relevant effects even at very low doses. The tested dose of 4 μg ml^{-1} of nickel sulphate ($NiSO_4 \cdot 6H_2O$) corresponds to more or less 1 ppm of Ni, dosage that is around the minimal sensitising threshold in already sensitised individuals with irritated skin. The concentration that is able to cause an allergic reaction in most of the sensitive subjects is anyway around higher value, over the 100 ppm of $NiSO_4 \cdot 6H_2O$ in contact with safe and intact skin.

The assay has been recognized as valid in compliance with the aforementioned method acceptance criteria, namely a percentage of living cells >80% tested by MTT assay (see Table SX in ESI†) and an MFI value of the $NiSO_4$ control (at the lower tested Ni concentration) >10% compared to the negative control with culture medium. The MFI must display a dose–response increasing pattern with the other two tested doses.

As the final result of the sensitisation assay in this *in vitro* model, the eluted samples do not affect the expression of the investigated markers in immunocompetent cells, and hence it does not show any stimulating potential on the immune cellular response mediated by monocytes/macrophages (Table S3†).

Conclusions

With the present work, we have been able to develop a new resin for stereolithography-based 3D printing with a bio-based content as high as 96.5% and by the employment of cheap components. The proposed inks offer a reliable green and low-cost alternative to oil-based formulations available on the market. The presented ink allows for the 3D printing of rigid structure with better mechanical resistance and lower fragility compared to most commercial equivalents, demonstrating that it is not required to lose performances when moving from fossil to bio-based sources. Moreover, the 3D printed object features good mechanical properties for applications in the textile industry; remarkably the elongation at break was 18%, which is higher than a recent manuscript based on the photocuring of similar methacrylates that did not contain a polyester component.[64] Biocompatibility has been checked confirming that no cytotoxicity or sensitisation stimulating immune cellular response are present. Taken together the last two features suggest a possible future focus on the development of DLP/SLA-based formulation of green textiles that would allow the employment of the reported formulation for the rapid prototyping of fashion products and accessories.[65] Finally, we demonstrated how it is possible to add functional components at very low percentage to the formulation without any influence on its printability, leading to functional 3D printed objects that reflect the physical–chemical properties of the additive.

Conflicts of interest

There are no conflicts to declare.

Acknowledgements

The University of Bologna is gratefully acknowledged.

Notes and references

1 I. Gibson, D. W. Rosen and B. Stucker, *Additive Manufacturing Technologies*, Springer US, 2010.
2 C. K. Chua, K. F. Leong and C. S. Lim, *Rapid Prototyping*, World Scientific, 2003.
3 A. L. Coats, J. P. Harrison, J. S. Hay and M. J. Ramos, 1503242A2, 2005.
4 L. Grigorian, 20190030792A1, 2019.
5 T. K. Dougherty, W. E. Elias, T. C. Thelander and M. N. Bhavnani, 5391460A, 1995.
6 J. S. Lee, 20140239527A1, 2014.
7 C. Baur, A. Askin, D. Cook, J. Giocondi, A. J. Skiles, S. Sullivan, R. Kniffel and J. T. Siemon, 20170322487A1, 2017.
8 M. Akutsu, T. Nakayashiki, H. Tachikawa, K. Ohkawa and S. Chikaoka, 5985510A, 1999.
9 Q. Ge, A. H. Sakhaei, H. Lee, C. K. Dunn, N. X. Fang and M. L. Dunn, *Sci. Rep.*, 2016, **6**, 31110.
10 A. J. Boydston, B. Cao, A. Nelson, R. J. Ono, A. Saha, J. J. Schwartz and C. J. Thrasher, *J. Mater. Chem. A*, 2018, **6**, 20621–20645.

11 B. Zhang, S. Li, H. Hingorani, A. Serjouei, L. Larush, A. A. Pawar, W. H. Goh, A. H. Sakhaei, M. Hashimoto, K. Kowsari, S. Magdassi and Q. Ge, *J. Mater. Chem. B*, 2018, **6**, 3246–3253.
12 D. K. Patel, A. H. Sakhaei, M. Layani, B. Zhang, Q. Ge and S. Magdassi, *Adv. Mater.*, 2017, **29**, 1606000.
13 S. Tibbits, *Archit. Des.*, 2014, **84**, 116–121.
14 Y. Shanjani, C. C. Pan, L. Elomaa and Y. Yang, *Biofabrication*, 2015, **7**, 045008.
15 G. Taormina, C. Sciancalepore, F. Bondioli and M. Messori, *Polymers*, 2018, **10**, 212.
16 Q. Mu, L. Wang, C. K. Dunn, X. Kuang, F. Duan, Z. Zhang, H. J. Qi and T. Wang, *Addit. Manuf.*, 2017, **18**, 74–83.
17 F. Wang, Y. Chong, F. K. Wang and C. He, *J. Appl. Polym. Sci.*, 2017, **134**, 1–8.
18 D. Zapfl, How 3D printing in the textile industry is leading into a new era, https://www.lead-innovation.com/english-blog/3d-printing-in-the-textile-industry, (accessed 15 July 2019).
19 E. Zolfagharifard, When science is stylish: Designer uses 3D printing to create a range of accessories that is taking the fashion world by storm, https://www.dailymail.co.uk/sciencetech/article-2384802/Catherine-Wales-uses-3D-printing-create-range-accessories-taking-fashion-world-storm.html, (accessed 15 July 2019).
20 S. Kim, H. Seong, Y. Her and J. Chun, *Fash. Text.*, 2019, **6**, 9.
21 E. Pei, J. Shen and J. Watling, *Rapid Prototyp. J.*, 2015, **21**, 556–571.
22 B. C. Gross, J. L. Erkal, S. Y. Lockwood, C. Chen and D. M. Spence, *Anal. Chem.*, 2014, **86**, 3240–3253.
23 C. Lu, C. Wang, J. Yu, J. Wang and F. Chu, *ChemSusChem*, 2020, **13**, 893–902.
24 J. T. Sutton, K. Rajan, D. P. Harper and S. C. Chmely, *ACS Appl. Mater. Interfaces*, 2018, **10**, 36456–36463.
25 N. B. Palaganas, J. D. Mangadlao, A. C. C. de Leon, J. O. Palaganas, K. D. Pangilinan, Y. J. Lee and R. C. Advincula, *ACS Appl. Mater. Interfaces*, 2017, **9**, 34314–34324.
26 J. Becker, A. Lange, J. Fabarius and C. Wittmann, *Curr. Opin. Biotechnol.*, 2015, **36**, 168–175.
27 T. Willke and K. D. Vorlop, *Appl. Microbiol. Biotechnol.*, 2001, **56**, 289–295.
28 S. Kumar, S. Krishnan, S. K. Samal, S. Mohanty and S. K. Nayak, *Polym. Int.*, 2017, **66**, 1349–1363.
29 M. Winkler, T. M. Lacerda, F. Mack and M. A. R. Meier, *Macromolecules*, 2015, **48**, 1398–1403.
30 D. G. Barrett, T. J. Merkel, J. C. Luft and M. N. Yousaf, *Macromolecules*, 2010, **43**, 9660–9667.
31 DataIntelo, *The Global Itaconic Acid Market by Applications (Synthetic Latex, Superabsorbent Polymers, Chelant Dispersant Agents, Unsaturated Polyester Resins, Methyl Methacrylate, and Detergent Builders) and Regions (Asia Pacific, North America, Latin America, Europe, and Middle East & Africa) – Global Industry Analysis, Growth, Share, Size, Trends and Forecast 2020–2026*, 2019.
32 H.-W. Lim, T. Cassidy and T. D. Cassidy, *Int. J. Eng. Technol.*, 2017, **9**, 78–83.
33 K. S. Lim, R. Levato, P. F. Costa, M. D. Castilho, C. R. Alcala-Orozco, K. M. A. van Dorenmalen, F. P. W. Melchels, D. Gawlitta, G. J. Hooper, J. Malda and T. B. F. Woodfield, *Biofabrication*, 2018, **10**, 034101.
34 M. S. Lowry, W. R. Hudson, R. A. Pascal and S. Bernhard, *J. Am. Chem. Soc.*, 2004, **126**, 14129–14135.
35 E. Matteucci, A. Baschieri, A. Mazzanti, L. Sambri, J. Ávila, A. Pertegás, H. J. Bolink, F. Monti, E. Leoni and N. Armaroli, *Inorg. Chem.*, 2017, **56**, 10584–10595.
36 Autodesk – Tinkercad, https://www.tinkercad.com/, (accessed 5 March 2019).
37 H. Biebl, K. Menzel, A. P. Zeng and W. D. Deckwer, *Appl. Microbiol. Biotechnol.*, 1999, **52**, 289–297.
38 G. Kaur, A. K. Srivastava and S. Chand, *Biochem. Eng. J.*, 2012, **64**, 106–118.
39 R. Ciriminna, C. Della Pina, M. Rossi and M. Pagliaro, *Eur. J. Lipid Sci. Technol.*, 2014, **116**, 1432–1439.
40 M. Fache, E. Darroman, V. Besse, R. Auvergne, S. Caillol and B. Boutevin, *Green Chem.*, 2014, **16**, 1987–1998.
41 H. Gong, M. Beauchamp, S. Perry, A. T. Woolley and G. P. Nordin, *RSC Adv.*, 2015, **5**, 106621–106632.
42 V. Somisetti, S. Allauddin, R. Narayan and K. V. S. N. Raju, *RSC Adv.*, 2015, **5**, 74003–74011.
43 Y. Kim, H. Watanabe, B. K. Kim and Y. B. Seu, *Tetrahedron: Asymmetry*, 2011, **22**, 1658–1661.
44 S. Alizadehgharib, A.-K. Östberg and U. Dahlgren, *Clin. Exp. Dent. Res.*, 2017, **3**, 227–234.
45 E. Yoshii, *J. Biomed. Mater. Res.*, 1997, **37**, 517–524.
46 J. Mokry, J. Karbanova, J. Lukas, V. Paleckova and B. Dvorankova, *Biotechnol. Prog.*, 2000, **16**, 897–904.
47 Y. Zhang, D. Chu, M. Zheng, T. Kissel and S. Agarwal, *Polym. Chem.*, 2012, **3**, 2752.
48 R. P. Johnson, Y.-I. Jeong, E. Choi, C.-W. Chung, D. H. Kang, S.-O. Oh, H. Suh and I. Kim, *Adv. Funct. Mater.*, 2012, **22**, 1058–1068.
49 K. Zhang, A. P. Woodruff, M. Xiong, J. Zhou and Y. K. Dhande, *ChemSusChem*, 2011, **4**, 1068–1070.
50 B. Pereira, H. Zhang, M. De Mey, C. G. Lim, Z. J. Li and G. Stephanopoulos, *Biotechnol. Bioeng.*, 2016, **113**, 376–383.
51 Y. Wang, M. Xian, X. Feng, M. Liu and G. Zhao, *Bioengineered*, 2018, **9**, 233–241.
52 H. Liu, K. R. M. Ramos, K. N. G. Valdehuesa, G. M. Nisola, W. K. Lee and W. J. Chung, *Appl. Microbiol. Biotechnol.*, 2013, **97**, 3409–3417.
53 J. Le Nôtre, S. C. M. Witte-van Dijk, J. van Haveren, E. L. Scott and J. P. M. Sanders, *ChemSusChem*, 2014, **7**, 2712–2720.
54 V. S. D. Voet, T. Strating, G. H. M. Schnelting, P. Dijkstra, M. Tietema, J. Xu, A. J. J. Woortman, K. Loos, J. Jager and R. Folkersma, *ACS Omega*, 2018, **3**, 1403–1408.
55 S. Kim, H. Seong, Y. Her and J. Chun, 4590301A, 1986.
56 J. P. Fouassier, F. Morlet-Savary, J. Lalevée, X. Allonas and C. Ley, *Materials*, 2010, **3**, 5130–5142.

57 J. Cantrell, S. Rohde, D. Damiani, R. Gurnani, L. DiSandro, J. Anton, A. Young, A. Jerez, D. Steinbach, C. Kroese and P. Ifju, in *Advancement of Optical Methods in Experimental Mechanics*, ed. L. Lamberti, M.-T. Lin, C. Furlong, C. Sciammarella, P. L. Reu and M. A. Sutton, Springer International Publishing, Cham, 2019, vol. 3.
58 Textile Innovation Knowledge Platform, http://www.tikp.co.uk/knowledge/material-functionality/luminescence/, (accessed 13 August 2019).
59 A. Auger, S. De Sousa Nobre and D. Getto, 20170089008A1, 2017.
60 J. M. Sanz Casado, R. Alcaraz De La Osa, F. Moreno Garcia, F. Gonzalez Fernandez, J. M. Saiz Vega, B. Aspeei, R. Gonzalez and Z. Martinez, 20170152627A1, 2017.
61 F. Dumur, D. Gigmes, J.-P. Fouassier and J. Lalevée, *Acc. Chem. Res.*, 2016, **49**, 1980–1989.
62 H. Huo, X. Shen, C. Wang, L. Zhang, P. Röse, L.-A. Chen, K. Harms, M. Marsch, G. Hilt and E. Meggers, *Nature*, 2014, **515**, 100–103.
63 A. Gualandi, E. Matteucci, F. Monti, A. Baschieri, N. Armaroli, L. Sambri and P. G. Cozzi, *Chem. Sci.*, 2017, **8**, 1613–1620.
64 J.-T. Miao, S. Peng, M. Ge, Y. Li, J. Zhong, Z. Weng, L. Wu and L. Zheng, *ACS Sustainable Chem. Eng.*, 2020, **8**, 9415–9424.
65 Julia Daviy – 3D Printed Fashion Designer – Sustainable Fashion, Fashion Innovation, https://juliadaviy.com/, (accessed 14 December 2019).